A Multiload Inductive Power Transfer Repeater System With Constant Load Current Characteristics

Chenwen Cheng, Fei Lu, *Member, IEEE*, Zhe Zhou, Weiguo Li, *Member, IEEE*, Chong Zhu, *Member, IEEE*, Zhanfeng Deng, Xi Chen, *Senior Member, IEEE*, and Chris Mi, *Fellow, IEEE*

***Abstract*— In this article, an inductive power transfer (IPT) system is designed to power multiple loads with nearly constant load currents using repeater coils. In the proposed IPT repeater system, every two repeater coils are grouped into a repeater unit and the load is connected to the first repeater coil in each repeater unit. It is deduced that the constant load current can be obtained when only considering the coupling coefficients between any two adjacent coils and omitting the coil resistances. Thus, the load power can be regulated independently, which greatly simplifies the power control design. A feasible magnetic structure is designed to meet the requirement that the coupling coefficients between the nonadjacent coils can be omitted. The relationship between the load resistances to achieve equal power distribution when considering coil resistances is derived. The proposed IPT system can be used to power gate drivers of the multiple submodules (SMs) that are connected in series in the modular multilevel converter (MMC). An experimental setup with six loads is constructed where the distance between two adjacent repeater units is 65 mm. The maximum system efficiency is around 60%.**

***Index Terms*— Dual coil design, equal power distribution, inductive power transfer (IPT), load independent, power repeater.**

I. Introduction

IN THE inductive power transfer (IPT) system, the efficiency depends on the coupling coefficient between coils and will drop dramatically with an increasing distance between the coils because their coupling coefficient decreases [1]. In order to increase the power transfer distance, additional resonant coils can be inserted between the transmitting and receiving coils, which function as power repeaters to enhance the magnetic field along the transmission path [2]–[10]. The traditional repeater coils are only used to increase the power transmission distance, and the load is only connected to the last receiving coil. Thus, the traditional IPT topology using repeater coils can only power one load. It is possible to connect the loads to the repeater coils, as discussed in [11]. In such a topology, the repeater coil not only transfers power to the next coil but also to the local load connected to it. However, the power obtained by one load will vary when other loads change. The loads that are far away from the transmitter even cannot receive enough power if the system parameters are not well designed. Thus, the load powers are coupled with each other, which increases the control design complexity.

Various compensation topologies have been studied for the IPT system, such as the series–series (SS) [12], series–parallel (SP) [13], parallel–series (PS) [14], parallel–parallel (PP) [14], LCC–LCC [15], and so on. The different compensation topologies not only increase the power transfer capability but also have some load-independent characteristics. For example, the load-independent output current in the secondary coil can be obtained for the SS compensation topology with a constant primary input voltage source if the compensation capacitances resonate with the self-inductances of the coils [16]. The load-independent constant current characteristic is obtained when neglecting the coil resistance, which greatly simplifies the power control. However, only one load exists in [16].

This article studies the load-independent characteristics in the long-distance IPT system using repeater coils for multiple loads. The repeater unit consisting of two repeater coils is designed, where the first coil is connected to a load. It is concluded that the constant load current can be obtained when only the coupling coefficients between any two adjacent coils are considered, while other couplings are neglected. In order to meet this requirement, a feasible magnetic design of the system is provided. The condition to achieve equal power distribution among all loads is derived when considering the coil resistances. The proposed IPT system can be used to power the multiple gate drivers of the submodules (SMs) in

Manuscript received December 10, 2018; revised June 20, 2019 and October 1, 2019; accepted October 27, 2019. Date of publication October 30, 2019; date of current version November 5, 2020. This work was supported by the Global Energy Interconnection Research Institute Company, Ltd (GEIRI) (State Grid Sci and Tech Project: Research on the Magnetic-Resonant Wireless Power Transfer Technology for the High-Voltage Converter Valve in FACTS) under Grant GEIRI-DL-71-17-011. Recommended for publication by Associate Editor Joseph O. Ojo. *(Corresponding author: Chris Mi.)*

C. Cheng and C. Mi are with the Department of Electrical and Computer Engineering, San Diego State University, San Diego, CA 92182 USA (e-mail: cheng.cwen@gmail.com; mi@ieee.org).

F. Lu is with the Department of Electrical and Computer Engineering, Drexel University, Philadelphia, PA 19104 USA (e-mail: fei.lu@drexel.edu).

Z. Zhou, W. Li, and Z. Deng are with the State Key Laboratory of Advanced Power Transmission Technology, Global Energy Interconnection Research Institute, Beijing 102211, China (e-mail: zhouzhe@geiri.sgcc.com.cn; lwgmb90549@sina.com; iphone21@sina.com).

C. Zhu is with the Department of Mechanical Engineering, Shanghai Jiao Tong University, Shanghai 200240, China (e-mail: chong.zhu@sjtu.edu.cn).

X. Chen is with the Global Energy Interconnection Research Institute North America, San Jose, CA 95134 USA (e-mail: xi.chen@geirina.net).

Color versions of one or more of the figures in this article are available online at http://ieeexplore.ieee.org.

Digital Object Identifier 10.1109/JESTPE.2019.2950609

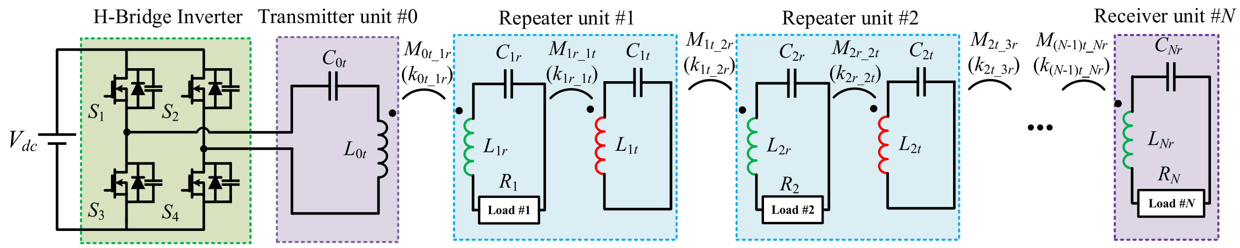

Fig. 1. Structure of the proposed IPT repeater system.

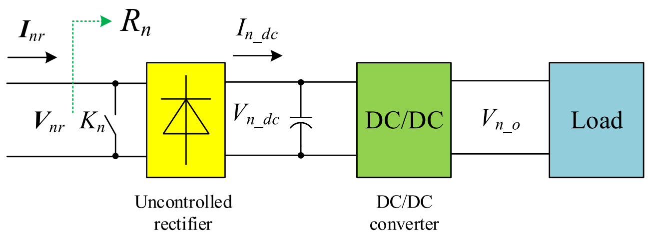

Fig. 2. Receiving circuit for unit #n.

a modular multilevel converter (MMC) [17], to balance the batteries' voltages in the battery management system [18] or to power multiple LEDs [19]. An experimental setup containing six loads is constructed to validate the effectiveness of the proposed IPT repeater system.

II. System Description and Analysis

A. System Structure

The structure of the proposed IPT repeater system for N loads is shown in Fig. 1. In order to provide power to multiple loads, the repeater units [unit #1 to #$(N-1)$] are designed. Each repeater unit consists of two repeater coils where the first coil receives power from its preceding coil and the second one transmits power to its subsequent coil. The number in the coil's subscript indicates the repeater unit, and the letter indicates whether the coil is a transmitting or receiving coil. For example, L_{1t} is the transmitting coil in unit #1. Since the coil connected to the inverter only transmits power to the other coils and the last coil only receives power from its preceding coil, they are noted as L_{0t} and L_{Nr}, respectively. C_{0t}, C_{1r}, C_{1t}, C_{2r}, $C_{2t}, \ldots, C_{Nr}$ are the compensation capacitances.

In practical applications, a receiving circuit should be designed for each load, which contains an uncontrolled rectifier and a dc/dc converter, as shown in Fig. 2. The rectifier transforms the received ac power into a dc source. Then, the dc/dc converter is used to regulate the load power and generate a stable dc output for the real load. A switch K_n is connected before the rectifier in the receiving circuit to protect the circuit. When the system works normally, K_n is open; once the failure is detected, K_n should be closed to cut off the receiving circuit and provide a pass for the constant current. Since the voltage across the rectifier and the current flowing into the rectifier are in phase, the receiving circuit can be regarded as resistive. Thus, R_n $(n = 1, 2, \ldots, N)$ is used to represent the equivalent load in the following context for simplification. M is the mutual inductance between two coils that are indicated by its subscript. For example, M_{1r_1t} is the mutual inductance between L_{1r} and L_{1t}. Similarly, k is the corresponding coupling coefficient, which can be calculated as

$$k_{i\_j} = M_{i\_j}/\sqrt{L_i \cdot L_j} \tag{1}$$

where i and j indicate the coil numbers.

B. System Modeling

The fundamental harmonics approximation (FHA) method is used to model the system and the circuit of the proposed IPT repeater system is shown in Fig. 3 where the mutual inductance model is adopted. $I_{0t}, I_{1r}, I_{1t}, I_{2r}, I_{2t}, \ldots, I_{Nr}$ are the currents flowing through $L_{0t}, L_{1r}, L_{1t}, L_{2r}, L_{2t}, \ldots, L_{Nr}$ respectively. The positive directions of these currents are defined when the currents flowing into the dot terminals of these coils. r_{0t}, r_{1r}, r_{1t}, r_{2r}, $r_{2t}, \ldots, r_{Nr}$ are the resistances of the corresponding coils. ω_0 is the operational angular frequency of the system. V_0 is the root mean square (rms) value of the fundamental component of the inverter's output voltage, which can be calculated as

$$V_0 = 2\sqrt{2} \cdot V_{\mathrm{dc}}/\pi. \tag{2}$$

When only the coupling coefficients between every two adjacent coils are considered and the other coupling effects are omitted, the voltage equation of each coil loop can be obtained using Kirchhoff's voltage law based on Fig. 3, which is shown as

$$\begin{bmatrix} \boldsymbol{V}_0 \\ 0 \\ 0 \\ \ldots \\ 0 \end{bmatrix} = \begin{bmatrix} Z_{0t} & j\omega_0 M_{0t\_1r} & 0 & \ldots & 0 \\ j\omega_0 M_{1r\_0t} & Z_{1r} & j\omega_0 M_{1r\_1t} & \ldots & 0 \\ 0 & j\omega_0 M_{1t\_1r} & Z_{1t} & \ldots & 0 \\ \ldots & \ldots & \ldots & \ldots & \ldots \\ 0 & 0 & 0 & \ldots & Z_{Nr} \end{bmatrix} \cdot \begin{bmatrix} \boldsymbol{I}_{0t} \\ \boldsymbol{I}_{1r} \\ \boldsymbol{I}_{1t} \\ \ldots \\ \boldsymbol{I}_{Nr} \end{bmatrix} \tag{3}$$

where $Z_{0t} = r_{0t} + j(\omega_0 L_{0t} - 1/\omega_0 C_{0t})$, $Z_{1r} = R_1 + r_{1r} + j(\omega_0 L_{1r} - 1/\omega_0 C_{1r})$ and $Z_{1t} = r_{1t} + j(\omega_0 L_{1t} - 1/\omega_0 C_{1t}), \ldots, Z_{Nr} = R_N + r_{Nr} + j(\omega_0 L_{Nr} - 1/\omega_0 C_{Nr})$.

C. Constant Load Currents

The compensation capacitances C_{0t}, C_{1r}, C_{1t}, C_{2r}, $C_{2t}, \ldots, C_{Nr}$ are designed to resonate with L_{0t}, L_{1r}, L_{1t},

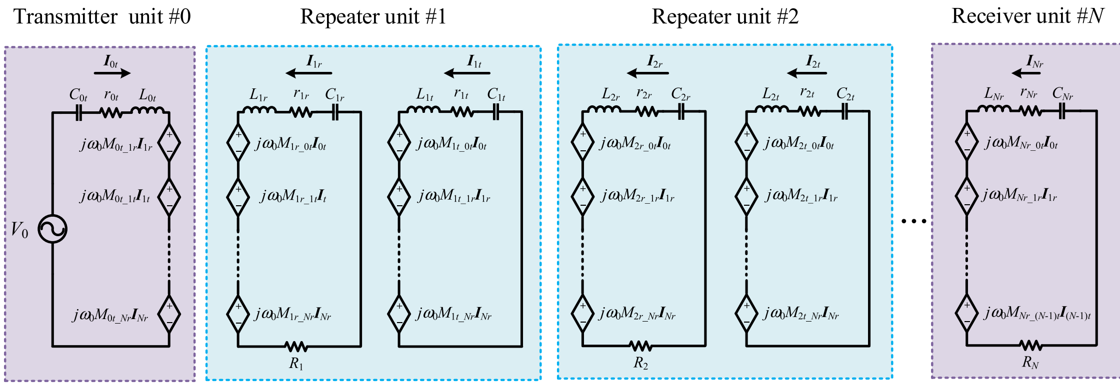

Fig. 3. Circuit model of the proposed IPT repeater system.

L_{2r}, $L_{2t}, \ldots, L_{Nr}$, respectively, as shown in the following equation:

$$\omega_0 = \frac{1}{\sqrt{L_{0t} \cdot C_{0t}}} = \frac{1}{\sqrt{L_{1r} \cdot C_{1r}}} = \frac{1}{\sqrt{L_{1t} \cdot C_{1t}}} = \cdots = \frac{1}{\sqrt{L_{Nr} \cdot C_{Nr}}}. \tag{4}$$

First, the coils' resistances are omitted, and the influence will be analyzed later. Substituting (4) into (3), the load currents can be calculated as

$$\begin{cases} \boldsymbol{I}_{1r} = \boldsymbol{V}_0 / j\omega_0 M_{0t\_1r} \\ \boldsymbol{I}_{2r} = -M_{1r\_1t} \cdot \boldsymbol{I}_{1r} / M_{1t\_2r} \\ \boldsymbol{I}_{3r} = -M_{2r\_2t} \cdot \boldsymbol{I}_{2r} / M_{2t\_3r} \\ \quad \cdots \\ \boldsymbol{I}_{Nr} = -M_{(N-1)r\_(N-1)t} \cdot \boldsymbol{I}_{(N-1)r} / M_{(N-1)t\_Nr}. \end{cases} \tag{5}$$

As can be seen from (5), the load current is independent of the load resistance R_n ($n = 1, 2, 3, \ldots, N$), which means that the load will not affect the load current when neglecting the resistances. Thus, the load power can be flexibly adjusted without affecting each other. When the input voltage $\boldsymbol{V}_0$ is fixed, the load currents are determined by the mutual inductances between the adjacent coils. Especially, the amplitudes of the load currents are identical if all the mutual inductances between the adjacent coils are the same, that is

$$M_{0t\_1r} = M_{1r\_1t} = M_{1t\_2r} = M_{2r\_2t} = \cdots = M_{(N-1)t\_Nr} = M. \tag{6}$$

It should be pointed out that even if (6) is not satisfied, when the mutual inductances between the adjacent two coils are different, the load currents are still independent of the load resistances but with different amplitudes. In this article, the IPT system that satisfies (6) will be analyzed because the identical load current facilitates the modular design of each of the repeater units and the receiving circuits.

D. Power Flow

When (6) is satisfied, the induced voltage $\boldsymbol{V}_{1t}$, $\boldsymbol{V}_{2t}$, $\boldsymbol{V}_{3t}$, $\boldsymbol{V}_{4t}, \ldots$, in L_{1t}, L_{2t}, L_{3t}, $L_{4t} \ldots$ by the currents flowing

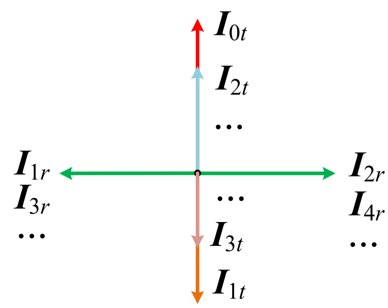

Fig. 4. Spatial vector relationship among the coil currents.

through their preceding load-connected coils $\boldsymbol{I}_{1r}$, $\boldsymbol{I}_{2r}$, $\boldsymbol{I}_{3r}$, $\boldsymbol{I}_{4r} \ldots$, respectively, can be calculated as

$$\begin{cases} \boldsymbol{V}_{1t} = j\omega_0 M \boldsymbol{I}_{1r} = \boldsymbol{V}_0 \\ \boldsymbol{V}_{2t} = j\omega_0 M \boldsymbol{I}_{2r} = -\boldsymbol{V}_0 \\ \boldsymbol{V}_{3t} = j\omega_0 M \boldsymbol{I}_{3r} = \boldsymbol{V}_0 \\ \quad \cdots \end{cases} \tag{7}$$

As can be seen from (7), the amplitudes of these voltages are $|\boldsymbol{V}_0|$ and the phase differences of the adjacent induced voltage vectors in nonload connected coils are always 180°.

Then, the currents in L_{1t}, $L_{2t}, \ldots, L_{(N-1)t}$ can also be calculated from (3) as

$$\begin{cases} \boldsymbol{I}_{(N-1)t} = -R_N \cdot \boldsymbol{I}_{Nr} / (j\omega_0 M) \\ \boldsymbol{I}_{(N-2)t} = -\boldsymbol{I}_{(N-1)t} - R_{N-1} \cdot \boldsymbol{I}_{(N-1)r} / (j\omega_0 M) \\ \quad \cdots \\ \boldsymbol{I}_{1t} = -\boldsymbol{I}_{2t} - R_2 \cdot \boldsymbol{I}_{2r} / (j\omega_0 M) \\ \boldsymbol{I}_{0t} = -\boldsymbol{I}_{1t} - R_1 \cdot \boldsymbol{I}_{1r} / (j\omega_0 M). \end{cases} \tag{8}$$

According to (5), the phase difference between the adjacent load currents is 180°. It can be found that the phase difference between the currents flowing through two adjacent nonload coils is also 180° based on (8). Moreover, the amplitudes of the currents flowing through nonload coils depend on the values of the load resistances. Also, the following inequality can be obtained according to (8):

$$|\boldsymbol{I}_{0t}| > |\boldsymbol{I}_{1t}| > |\boldsymbol{I}_{2t}| > \cdots > |\boldsymbol{I}_{(N-1)t}|. \tag{9}$$

Fig. 4 shows the spatial vector relationship among all the coil currents. Each coil current lags the current flowing through its preceding coil 90°. Amplitudes of the currents in load-connected coils are identical, while those of the currents in nonload connected coils decrease as the transmitting distance increases.

The input power of the system can be calculated using (7) and (8) as

$$\begin{aligned} P_{\text{in}} &= \text{Re}[\boldsymbol{V}_0 \cdot \hat{\boldsymbol{I}}_{0t}] = \underbrace{\text{Re}[\boldsymbol{V}_0 \cdot (-\hat{\boldsymbol{I}}_{1t})]}_{P_{1t}} + \underbrace{|\boldsymbol{I}_{1r}|^2 \cdot R_1}_{P_{R1}} \\ &= \underbrace{\text{Re}[\boldsymbol{V}_0 \cdot (\hat{\boldsymbol{I}}_{2t})]}_{P_{2t}} + \underbrace{|\boldsymbol{I}_{2r}|^2 \cdot R_2}_{P_{R2}} + \underbrace{|\boldsymbol{I}_{1r}|^2 \cdot R_1}_{P_{R1}} \\ &= \cdots \\ &= \sum_{n=1}^{N} P_{Rn} \end{aligned} \tag{10}$$

where P_{Rn} $(n = 1, 2, \ldots N)$ is the power consumed by the nth load resistance R_n.

III. Influence of Coil Resistances

A. Load Currents

As analyzed earlier, the constant load current can be obtained in the proposed multiload IPT system when neglecting the coil resistances. However, the resistances are inevitable in a practical system. The quality factors of L_{0t}, L_{1r}, $L_{1t}, \ldots, L_{Nr}$ are defined as Q_{0t}, Q_{1r}, $Q_{1t}, \ldots, Q_{Nr}$, respectively. Thus, the coil resistances can be calculated as

$$r_i = \omega_0 L_i / Q_i \tag{11}$$

where the subscript i indicates the coil number.

In order to analyze the load current, the reflected impedance is used [22], which is defined as the equivalent impedance that represents the influence of all the subsequence coils on the designated coil. For the repeater unit #n, the reflected impedances in the two coils can be calculated as

$$\begin{cases} Z_{r,nt} = \dfrac{(\omega_0 M_{nt\_(n+1)r})^2}{(r_{(n+1)r} + R_{n+1} + Z_{r,(n+1)r})}, \\ \qquad\qquad n = 0, 1, 2, \ldots, N-1 \\ Z_{r,nr} = (\omega_0 M_{nr\_nt})^2 / (r_{nt} + Z_{r,nt}), \\ \qquad\qquad n = 1, 2, 3, \ldots, N-1. \end{cases} \tag{12}$$

Because there is no coil after the receiver unit #N, the reflected impedance in L_{Nr} is zero, i.e., $Z_{r,Nr} = 0$. Thus, the different load currents can be calculated as

$$\begin{cases} \boldsymbol{I}_{0t} = \boldsymbol{V}_0 / (r_{0t} + Z_{r,0t}) \\ \boldsymbol{I}_{nr} = -j\omega_0 M_{(n-1)t\_nr} \boldsymbol{I}_{(n-1)t} / (r_{nr} + R_n + Z_{r,nr}), \\ \qquad\qquad n = 1, 2, \ldots, N \\ \boldsymbol{I}_{nt} = -j\omega_0 M_{nr\_nt} \boldsymbol{I}_{nr} / r_{nt} + Z_{r,nt}, \quad n = 1, 2, \ldots, N-1. \end{cases} \tag{13}$$

When all the coils are designed identically, the quality factors and the resistances of these coils are also the same, that is

$$Q_{0t} = Q_{1r} = Q_{1t} = \cdots = Q_{Nr} = Q \tag{14}$$

$$r_{0t} = r_{1r} = r_{1t} = \cdots = r_{Nr} = r. \tag{15}$$

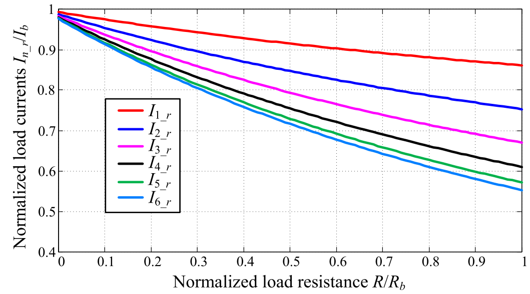

Fig. 5. Load current variations with increasing load resistance ($k = 0.1$ and $Q = 300$).

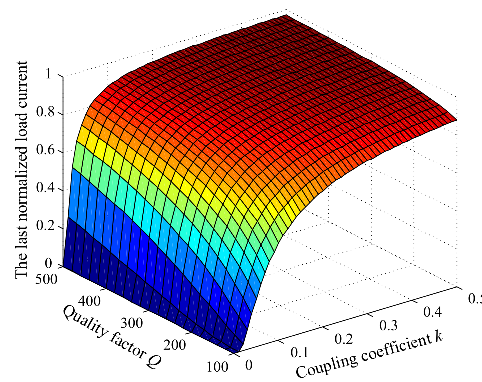

Fig. 6. Last load current variation with different coupling coefficients and quality factors ($R/R_b = 0.3$).

When (6) is satisfied, the coupling coefficients between every two adjacent coils are identical, that is

$$k_{0t\_1r} = k_{1r\_1t} = k_{1t\_2r} = k_{2r\_2t} = \cdots = k_{(N-1)t\_Nr} = k. \tag{16}$$

Based on (12)–(16), Fig. 5 shows the load current variations against the load resistance, where $N = 6$, $k = 0.1$, and $Q = 300$. In Fig. 5, all the load resistances are identical, that is

$$R_1 = R_2 = \cdots = R_N = R. \tag{17}$$

In order to facilitate the comparison between different load currents, the load resistances and currents are divided by their base values that are defined as

$$R_b = \omega_0 M, \quad I_b = V_0 / R_b. \tag{18}$$

It can be seen that the load currents decrease gradually in a practical system considering the coils' resistances when the load resistance R increases. It can be seen that the decreasing rates of these load currents are different. The longer the distance between the load-connected coil and L_{0t}, the faster the load current decays.

Since the last load current drops the most, the variation of the last load current can be regarded as a criterion for evaluating the constant current characteristics of the whole system. Fig. 6 shows the last load current variation with different coupling coefficients and quality factors when $R/R_b = 0.3$. A larger coupling coefficient k or quality factor Q leads to

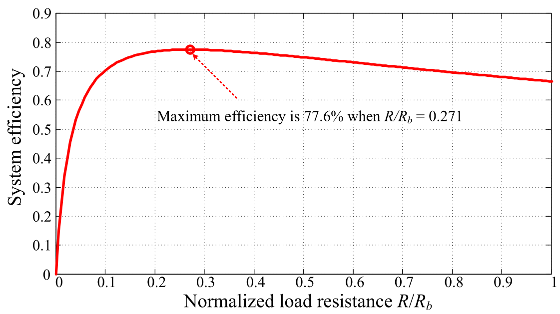

Fig. 7. System efficiency variation against the load resistance ($N = 6$, $k = 0.1$, and $Q = 300$).

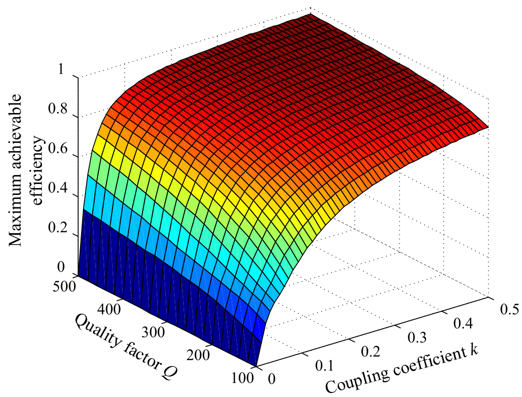

Fig. 8. Maximum achievable efficiency with different coupling coefficients and quality factors ($N = 6$).

less current drop, which means that a better constant load-independent current characteristic can be obtained.

B. System Efficiency

In the proposed IPT repeater system, the total output power is defined as the sum of the power consumed by all the loads, which is expressed as

$$P_o = \sum_{n=1}^{N} I_{nr}^2 \cdot R_n. \tag{19}$$

The input power is written as

$$P_{\text{in}} = \text{Re}(\boldsymbol{V}_0 \cdot \hat{\boldsymbol{I}}_{0t}) \tag{20}$$

where Re(X) represents the real part of “X” and “^” represents the conjugate value. Then, the system efficiency can be expressed as

$$\eta = P_o / P_{\text{in}}. \tag{21}$$

Based on (12)–(21), Fig. 7 shows the variation of the system efficiency against the load resistance where $N = 6$, $k = 0.1$, and $Q = 300$. As can be seen, the maximum efficiency is 77.6%, which is achieved when the normalized load resistance is 0.271. The maximum achievable efficiency depends on k and Q. The variation of the maximum achievable efficiency against k and Q when $N = 6$ is shown in Fig. 8. When k or Q becomes larger, the maximum achievable efficiency is also higher.

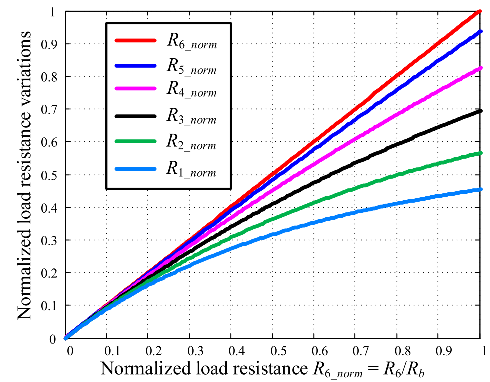

Fig. 9. Load resistances’ variations to achieve equal power distribution among all the loads ($N = 6$, $k = 0.1$, and $Q = 300$).

C. Equal Power Distribution

If the loads connected to the IPT system are identical, nearly equal amount of power is consumed by each load during normal working conditions. Thus, the condition to achieve equal power distribution among all the loads is studied.

When considering the coil resistances, some power is consumed by the resistances so that equal power cannot be obtained with the same load resistance. The ratio between the power consumed on the adjacent load resistances R_n and R_{n+1} is defined as λ_n, which can be calculated as follows:

$$\lambda_n = \frac{P_{R(n+1)}}{P_{Rn}} = \frac{Z_{r,nr}}{R_n} \cdot \frac{Z_{r,nt}}{r_{nt} + Z_{r,nt}} \cdot \frac{R_{n+1}}{R_{n+1} + r_{(n+1)r} + Z_{r,(n+1)r}} \quad n = 1, 2, \ldots, N-1. \tag{22}$$

In order to achieve equal power distribution among all the loads, λ_n should be equal to 1 when n varies from 1 to $N - 1$. Fig. 9 shows the load resistance variations when the sixth load resistance R_6 increases to achieve equal power distribution among all the loads where $N = 6$, $k = 0.1$, and $Q = 300$. The load resistances have been normalized by dividing the base resistance R_b as defined in (18). As R_{6_norm} increases, the difference between all the six loads becomes larger, which means that the difference between the load currents is larger as the output power increases. This is because the amplitudes of currents flowing through nonload connected coils, i.e., $\boldsymbol{I}_{0t}$, $\boldsymbol{I}_{1t}$, $\boldsymbol{I}_{2t}$ ..., increase when the load resistances increase, as shown in (8). Thus, more power loss is produced and the load current differences become larger.

IV. Magnetic Coupler Design

In order to obtain the load-independent load current characteristics, special magnetic coupling conditions should be met, which requires that the coupling coefficients between the nonadjacent coils can be omitted as discussed earlier. Moreover, the two coils in the same repeater unit should be placed close to save space. In this section, the double-D coils are used [20], [21]. Fig. 10 shows the double-D coils in two different directions. In Fig. 10(a), the magnetic field generated by the double-D coil is along the x-axis, while in Fig. 10(b), the magnetic field is along the y-axis. When the two double-D coils are placed perpendicularly and coaxially, their magnetic fields will also be orthogonal. It means that the magnetic

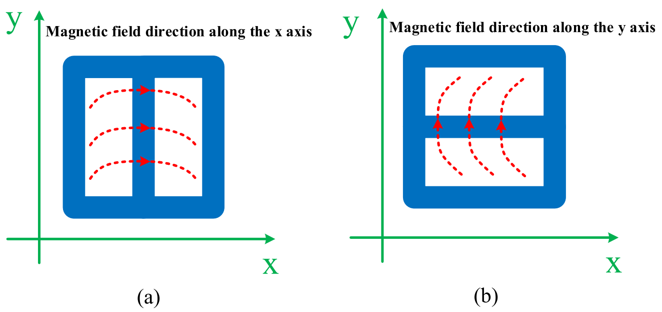

Fig. 10. Magnetic field patterns of the double-D coils in two different directions. Magnetic field along the (a) x-axis, and (b) y-axis.

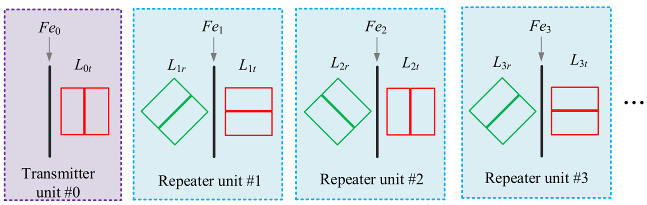

Fig. 11. Coil structure for the proposed IPT repeater system.

fields generated by these two double-D coils will be decoupled from each other and their magnetic coupling can be neglected. Such a feature can be used in the coil design to eliminate the undesirable coupling between the nonadjacent coils. A feasible magnetic structure is designed, as shown in Fig. 11. Taking repeater units #1 and #2 as an example, only the magnetic couplings between L_{1r} and L_{1t}, L_{1t} and L_{2r}, and L_{2r} and L_{2t} are desirable, while the couplings between L_{1r} and L_{2r}, L_{1r} and L_{2t}, and L_{1t} and L_{2t} should be as small as possible. In order to remove the coupling coefficient between L_{1r} and L_{2r}, these two coils are placed perpendicularly. Similarly, L_{1t} and L_{2t} are also placed perpendicularly. Considering that L_{1t} should be coupled with both L_{1r} and L_{2r}, L_{1t} can be rotated by an angle of θ compared to L_{1r}. Since L_{2t} is perpendicular to L_{1t}, L_{2t} should be rotated by an angle of $(90° + \theta)$ compared to L_{1r}. θ should be greater than 0° and smaller than 90°. In this article, θ is chosen as 45° for symmetry so that all coils are rotated by 45° compared to its previous one.

The ferrite plates (Fe_0, Fe_1, Fe_2, $Fe_3, \ldots$) are inserted not only between the two coils in the repeater unit but also beside the coils in the transmitter unit #0 and receiver unit #N. Moreover, the coupling coefficients between L_{1r} and L_{2t} or the coils following L_{2t} can also be omitted because their distances are long enough and the ferrites between them can also insulate the magnetic fields.

The 3-D simulation model using MAXWELL is shown in Fig. 12. The distance between the adjacent units is $d = 65$ mm. All the coils are square with the side length $l_{\text{coil}} = 140$ mm and the width of the coils is $l_w = 16$ mm. The ferrite plates are also square with the side length $l_{\text{fe}} = 150$ mm. In order to achieve an equal coupling coefficient between two adjacent coils, a square hole is designed in every ferrite plate whose side length is defined as l_{hole}.

Fig. 13 shows the influence of the ferrite plate's thickness on the coupling coefficient between the repeater coils. Because of the system symmetric characteristics, only units #1 and #2 are considered. The solid, dashed, and dotted lines represent the simulation results when the thicknesses are 1, 3, and 5 mm, respectively. When the thickness becomes larger, the distance between the two coils in the same repeater units will also be increased so that the coupling coefficient between them is smaller with the same hole size. Moreover, in order to achieve equal coupling coefficient between any two adjacent coils, the hole size should be larger with a thinner ferrite plate. Taking the 1-mm-thickness ferrite plate as an example, k_{1r_1t} increases as the hole becomes larger, while k_{1t_2r} decreases. k_{1r_2r} and k_{1r_2t} keep low when the hole size changes as explained earlier. Based on the simulation results, when the side length of the hole l_{hole} is 50 mm, nearly identical coupling coefficient between every two adjacent coils, which is 0.065 in this case, can be obtained. Meanwhile, k_{1r_2t} is about 0.003 and k_{1r_2r} is about 0.000008, which can be neglected compared to k_{1r_1t} or k_{1t_2r}.

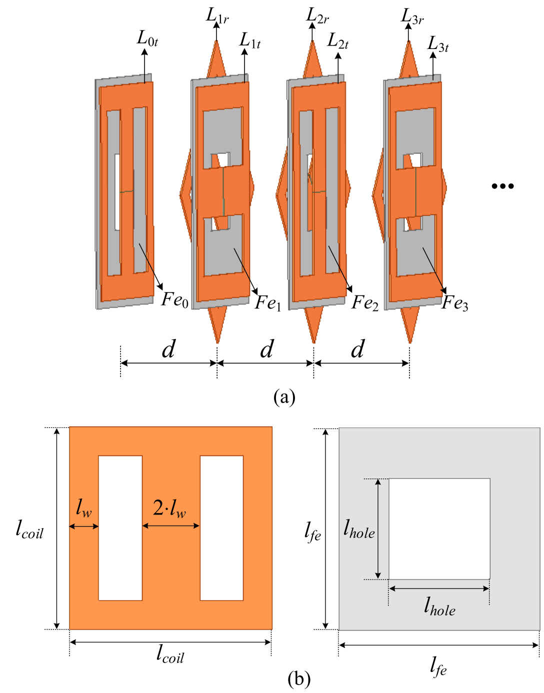

Fig. 12. FEA simulation model of the designed coil structure. (a) FEA simulation model. (b) Coil and ferrite dimensions.

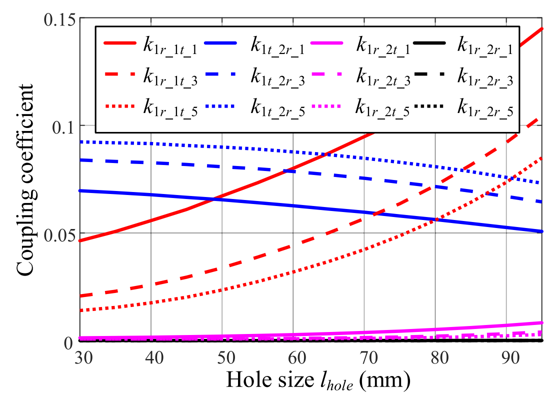

Fig. 13. Coupling coefficient variation with different hole sizes and ferrite thicknesses.

(a)

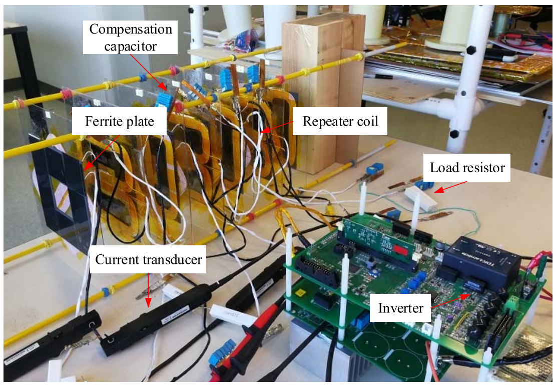

(b)

Fig. 14. Experimental system. (a) Coil structure. (b) Experimental setup.

TABLE I
PARAMETERS OF THE DESIGNED EXPERIMENTAL PROTOTYPE

Parameter	Value	Parameter	Value
V_{dc}	10V	f_s	300kHz
l_{coil}	140mm	l_{fe}	150mm
l_w	16mm	d	65mm
N	6	l_{hole}	50mm
Ferrite thickness	1mm	$L_{0\_t} \sim L_{6\_r}$	90μH
$C_{0\_t} \sim C_{6\_r}$	3.13nF	k	0.06
r	0.67Ω	Q	250

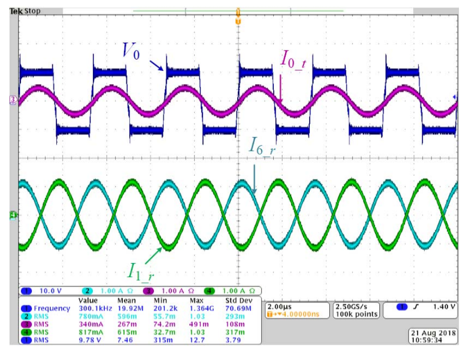

Fig. 15. Experimental waveform of the input voltage and load currents.

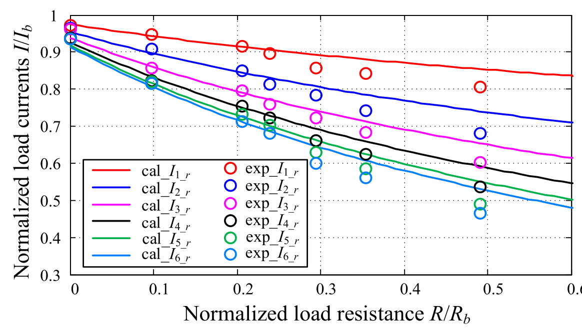

Fig. 16. Load current variation with increasing load resistance R/R_b.

V. EXPERIMENTAL RESULTS

A. Experimental Prototype

An experiment prototype with six loads has been designed to validate the proposed IPT system in this article, as shown in Fig. 14. The coils are made of 300 strand litz wires with a diameter of 0.05 mm. The dimension of the coil is 140 mm × 140 mm with the turn number of 12. The 150 mm × 150 mm ferrite plate of 1 mm thickness is designed with a 50 mm × 50 mm hole. Four silicon carbide MOSFETs (C2M0080120D) are used to form the inverter, and a high-frequency ac voltage source can be generated for the system. In the experimental platform, PC40 is adopted as the ferrite material, the optimal operating frequency of which is around 100–300 kHz. Although a high operational frequency is beneficial to reduce the coils' volume and the compensation capacitor values, higher losses will be generated in the ferrite plate as well as in the coil because of the skin and proximity effect. The maximum withstand voltage of the film capacitor that is used as the compensation capacitor will also drops as the operating frequency increases. Thus, the operating frequency cannot be too high; otherwise, the capacitor would be easily damaged. As a result, the operating frequency is chosen as 300 kHz.

The distance between the two adjacent units is 65 mm. The coupling coefficient of two adjacent coils is measured around 0.06, which is consistent with the abovementioned simulation results. The coupling coefficients k_{1r_2t} and k_{1r_2r} are measured as 0.003 and 0.001, respectively, which can be neglected when compared with k_{1r_1t} of 0.06. The quality factor of the resonant loop is measured as 250. The detailed circuit parameters are listed in Table I.

B. Load Current Characteristics

With the parameters listed in Table I, every coil resonates with its respective compensation capacitor. Fig. 15 shows the experimental waveform of the input voltage and current as well as the load currents $\boldsymbol{I}_{1\_r}$ and $\boldsymbol{I}_{6\_r}$. The phase of the input current $\boldsymbol{I}_{0\_t}$ lags slightly behind the input voltage $\boldsymbol{V}_0$ so that the zero-voltage switching (ZVS) of the MOSFETs can be obtained and the switching loss can be decreased. The first load current $\boldsymbol{I}_{1\_r}$ lags behind the input current $\boldsymbol{I}_{0\_t}$ by 90° and the sixth load current is in the opposite phase compared with $\boldsymbol{I}_{1\_r}$, which is consistent with the analysis in Fig. 4.

Fig. 16 shows that the load current decreases when the load resistance increases. The solid lines represent the calculated currents, while the dots represent the measured currents. The measured currents are consistent with the calculated values well. When the load resistance is large, the measured currents are a little lower than the calculated ones. It is because the voltage drop on the reactance of L_{0_t}, which is used to obtain ZVS for the MOSFETs, becomes larger when load power increases.

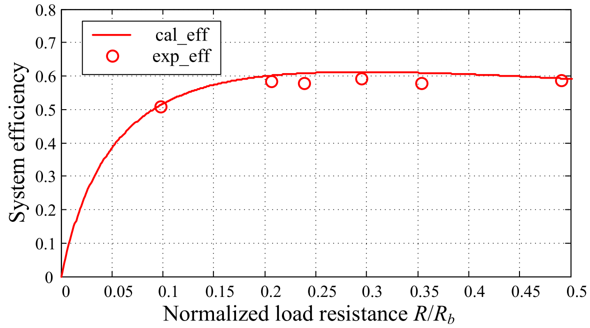

Fig. 17. Efficiency of the experimental setup.

TABLE II
GROUP OF LOAD RESISTANCE TO OBTAIN EQUAL POWER DISTRIBUTION

Load number	1	2	3	4	5	6
Resistance/Ω	2.50	3.43	4.48	5.86	7.19	8.01

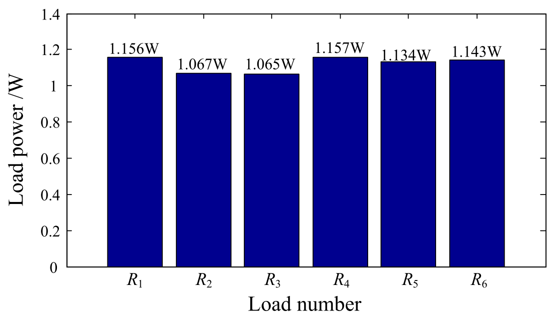

Fig. 18. Equal power distribution among all six loads.

C. System Efficiency

The efficiency of the experimental setup is shown in Fig. 17. The maximum experimental efficiency is 59.1% with $k = 0.06$ and $Q = 250$. The efficiency can be improved further with larger k or Q, which requires a larger coil size or new magnetic structure as long as the coupling coefficient between the nonadjacent coils can be neglected.

D. Equal Power Distribution

In order to obtain equal power distribution, (22) should be met, where $\lambda_n = 1$ $(n = 1, 2, \ldots, N - 1)$. A group of the six load resistances have been calculated based on (22), which is shown in Table II. Fig. 18 shows the power of the six loads when using the load resistances listed in Table II. The maximum load power is 1.157 W, and the minimum load power is 1.065 W. The power variation is within 5%. The load power is tested when the dc voltage V_{dc} of the inverter is 10 V, which will be higher when V_{dc} increases.

VI. CONCLUSION

In this article, a novel IPT system is designed to power multiple loads simultaneously. There are three contributions in this article as follows.

1) In order to power loads simultaneously, a dual-coil repeater structure is designed and the load is only connected to the first coil in each repeater unit. The load currents are independent of load variations when neglecting the coil resistances, which facilitate the control design.
2) A feasible magnetic structure example using repeater units is designed, which assumes that all loads are placed along a line over a long distance. Double-D coils are adopted, and the ferrite plate is inserted between the two coils in each unit, which is designed with a hole. Then, the coupling coefficients between the adjacent coils can be adjusted by changing the hole size. Such a magnetic design ensures that the coupling coefficients only exist between the adjacent coils.
3) Since usually equal power is consumed in each load, the condition to obtain equal power distribution among all the loads when considering the coil resistances is analyzed. A larger coupling coefficient k or quality factor Q is beneficial to decrease the load resistance difference to obtain equal power distribution.

The proposed IPT system is suitable for powering the gate drivers of the SMs in an MMC because high insulation level can be achieved. The effectiveness of the proposed IPT repeater system has been validated by experimental results.

REFERENCES

[1] Z. Zhang, H. Pang, A. Georgiadis, and C. Cecati, "Wireless power transfer—An overview," *IEEE Trans. Ind. Electron.*, vol. 66, no. 2, pp. 1044–1058, Feb. 2019.
[2] J. Alberto, U. Reggiani, L. Sandrolini, and H. Albuquerque, "Accurate calculation of the power transfer and efficiency in resonator arrays for inductive power transfer," *Prog. Electromagn. Res. B*, vol. 83, pp. 61–76, Feb. 2019, doi: 10.2528/PIERB18120406.
[3] C. J. Stevens, "Magnetoinductive waves and wireless power transfer," *IEEE Trans. Power Electron.*, vol. 30, no. 11, pp. 6182–6190, Nov. 2015.
[4] C. K. Lee, W. X. Zhong, and S. Y. R. Hui, "Effects of magnetic coupling of nonadjacent resonators on wireless power domino-resonator systems," *IEEE Trans. Power Electron.*, vol. 27, no. 4, pp. 1905–1916, Apr. 2012.
[5] K. Lee and S. H. Chae, "Power transfer efficiency analysis of intermediate-resonator for wireless power transfer," *IEEE Trans. Power Electron.*, vol. 33, no. 3, pp. 2484–2493, Mar. 2018.
[6] D. Ahn and S. Hong, "A study on magnetic field repeater in wireless power transfer," *IEEE Trans. Ind. Electron.*, vol. 60, no. 1, pp. 360–371, Jan. 2013.
[7] C. Zhang, D. Lin, N. Tang, and S. Y. R. Hui, "A novel electric insulation string structure with high-voltage insulation and wireless power transfer capabilities," *IEEE Trans. Power Electron.*, vol. 33, no. 1, pp. 87–96, Jan. 2018.
[8] C. Cai *et al.*, "Resonant wireless charging system design for 110-kV high-voltage transmission line monitoring equipment," *IEEE Trans. Ind. Electron.*, vol. 66, no. 5, pp. 4118–4129, May 2019.
[9] Y. Zhang, Z. Zhao, F. He, K. Chen, T. Lu, and L. Yuan, "Increasing power level of resonant wireless power transfer with relay resonators by considering resonator current amplitudes," in *Proc. IEEE Energy Convers. Congr. Exposit. (ECCE)*, Sep. 2015, pp. 3077–3081.
[10] W. X. Zhong, C. K. Lee, and S. Y. Hui, "Wireless power domino-resonator systems with noncoaxial axes and circular structures," *IEEE Trans. Power Electron.*, vol. 27, no. 11, pp. 4750–4762, Nov. 2012.
[11] F. Lu *et al.*, "A high-efficiency and long-distance power-relay system with equal power distribution," *IEEE J. Emerg. Sel. Topics Power Electron.*, to be published.
[12] H. Feng, T. Cai, S. Duan, X. Zhang, H. Hu, and J. Niu, "A dual-side-detuned series–series compensated resonant converter for wide charging region in a wireless power transfer system," *IEEE Trans. Ind. Electron.*, vol. 65, no. 3, pp. 2177–2188, Mar. 2018.
[13] W. Zhang, S.-C. Wong, C. K. Tse, and Q. Chen, "Analysis and comparison of secondary series- and parallel-compensated inductive power transfer systems operating for optimal efficiency and load-independent voltage-transfer ratio," *IEEE Trans. Power Electron.*, vol. 29, no. 6, pp. 2979–2990, Jun. 2014.

[14] J. L. Villa, J. Sallan, J. F. S. Osorio, and A. Llombart, "High-misalignment tolerant compensation topology for ICPT systems," *IEEE Trans. Ind. Electron.*, vol. 59, no. 2, pp. 945–951, Feb. 2012.

[15] S. Li, W. Li, J. Deng, T. D. Nguyen, and C. C. Mi, "A double-sided LCC compensation network and its tuning method for wireless power transfer," *IEEE Trans. Veh. Technol.*, vol. 64, no. 6, pp. 2261–2273, Jun. 2015.

[16] W. Zhang, S.-C. Wong, C. K. Tse, and Q. Chen, "Load-independent duality of current and voltage outputs of a series-or parallel-compensated inductive power transfer converter with optimized efficiency," *IEEE J. Emerg. Sel. Topics Power Electron.*, vol. 3, no. 1, pp. 137–146, Mar. 2015.

[17] M. Takasaki, Y. Miura, and T. Ise, "Wireless power transfer system for gate power supplies of modular multilevel converters," in *Proc. IEEE Int. Power Electron. Motion Control Conf. (ECCE Asia)*, May 2016, pp. 3183–3190.

[18] M. Liu, M. Fu, Y. Wang, and C. Ma, "Battery cell equalization via megahertz multiple-receiver wireless power transfer," *IEEE Trans. Power Electron.*, vol. 33, no. 5, pp. 4135–4144, May 2014.

[19] X. Qu, W. Zhang, S.-C. Wong, and C. K. Tse, "Design of a current-source-output inductive power transfer LED lighting system," *IEEE J. Emerg. Sel. Topics Power Electron.*, vol. 3, no. 1, pp. 306–314, Mar. 2015.

[20] M. Budhia, J. T. Boys, G. A. Covic, and C.-Y. Huang, "Development of a single-sided flux magnetic coupler for electric vehicle IPT charging systems," *IEEE Trans. Ind. Electron.*, vol. 60, no. 1, pp. 318–328, Jan. 2013.

[21] T. Kan, F. Lu, T.-D. Nguyen, P. P. Mercier, and C. C. Mi, "Integrated coil design for EV wireless charging systems using LCC compensation topology," *IEEE Trans. Power Electron.*, vol. 33, no. 11, pp. 9231–9241, Nov. 2018.

[22] J. Alberto, U. Reggiani, L. Sandrolini, and H. Albuquerque, "Fast calculation and analysis of the equivalent impedance of a wireless power transfer system using an array of magnetically coupled resonators," *Prog. Electromagn. Res. B*, vol. 80, pp. 101–112, Apr. 2018, doi: 10.2528/PIERB18011704.

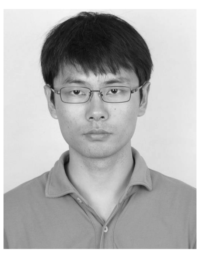

Chenwen Cheng received the B.S. and Ph.D. degrees from Zhejiang University, Hangzhou, China, in 2012 and 2017, respectively, all in electrical engineering.

He is currently a Post-Doctoral Researcher with San Diego State University, San Diego, CA, USA. His current research interests include motor control, renewable power generation, and wireless power transfer technologies.

Fei Lu (S'12–M'17) received the B.S. and M.S. degrees from the Harbin Institute of Technology, Harbin, China, in 2010 and 2012, respectively, and the Ph.D. degree from the University of Michigan, Ann Arbor, MI, USA, in 2017, all in electrical engineering.

He is currently an Assistant Professor with the Department of Electrical and Computer Engineering, Drexel University, Philadelphia, PA, USA. His current research interests include power electronics and the application of electric vehicle charging.

Zhe Zhou received the B.E. degree in measure and control technology and instrumentations from the Changchun University of Science and Technology, Changchun, China, in 2011, and the M.S. degree in power electronics and power drives from Tianjin University, Tianjin, China, in 2014.

He is currently with the State Key Laboratory of Advanced Power Transmission Technology, Global Energy Interconnection Research Institute, Beijing, China. His current research interests include the applications of the widegap devices and the power electronic transformer.

Weiguo Li (M'01) received the B.S. degree from Northeast Dianli University, Jilin, China, in 1996, the M.S. degree from China Electric Power Research Institute, Beijing, China, in 2006, and the Ph.D. degree from North China Electric Power University, Beijing, in 2013, all in electrical engineering.

He is currently with the State Key Laboratory of Advanced Power Transmission Technology, Global Energy Interconnection Research Institute, Beijing. His current research interests include the flexible ac transmission systems and power systems.

Chong Zhu (M'17) received the B.S. degree in electrical engineering from the China University of Mining and Technology, Xuzhou, China, in 2010, and the Ph.D. degree in electrical engineering from Zhejiang University, Hangzhou, China, in 2016.

From 2017 to 2019, he was a Post-Doctoral Researcher with San Diego State University, San Diego, CA, USA. He is currently an Assistant Professor with the School of Mechanical Engineering, Shanghai Jiao Tong University, Shanghai, China. His current research interests include battery thermal management and power electronics applied in electric vehicles.

Zhanfeng Deng received the B.S. and M.S. degrees in welding technology and equipment from Jilin Polytechnical University, Changchun, China, in 1996, and the Ph.D. degree in electrical engineering from Tsinghua University, Beijing, China, in 2003.

He is currently with the State Key Laboratory of Advanced Power Transmission Technology, Global Energy Interconnection Research Institute, Beijing. His current research interests include flexible ac transmission systems and power systems.

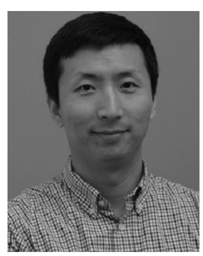

Xi Chen (S'07–M'13–SM'16) received the B.Eng. degree in information engineering from Beijing Technology and Business University, Beijing, China, in 2003, the M.Sc. degree in digital signal processing from Kings College London, University of London, London, U.K., in 2005, and the Ph.D. degree in electronic and information engineering from The Hong Kong Polytechnic University, Hong Kong, in 2009.

In 2014, he joined the Global Energy Interconnection Research Institute North America, San Jose, CA, USA, where he is currently the Chief Information Officer. His current research interests include the Internet of Things, smart grid, electric vehicle charging infrastructure, and complex networks analysis and its applications.

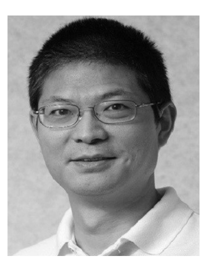

Chris Mi (S'00–A'01–M'01–SM'03–F'12) received the B.S.E.E. and M.S.E.E. degrees in electrical engineering from Northwestern Polytechnical University, Xi'an, China, in 1985 and 1988, respectively, and the Ph.D. degree in electrical engineering from the University of Toronto, Toronto, ON, Canada, in 2001.

From 2001 to 2015, he was with the University of Michigan, Dearborn, MI, USA. He is currently a Professor and the Chair of electrical and computer engineering and the Director of the Department of Energy (DOE)-funded Graduate Automotive Technology Education (GATE) Center for Electric Drive Transportation, San Diego State University, San Diego, CA, USA.